JCTC Journal of Chemical Theory and Computation

Article

pubs.acs.org/JCTC

Double-Ended Surface Walking Method for Pathway Building and Transition State Location of Complex Reactions

Xiao-Jie Zhang, Cheng Shang, and Zhi-Pan Liu*

Shanghai Key Laboratory of Molecular Catalysis and Innovative Materials, Key Laboratory of Computational Physical Science (Ministry of Education), Department of Chemistry, Fudan University, Shanghai 200433, China

ABSTRACT: Toward the activity prediction with large-scale computations, here a double-ended surface walking (DESW) method is developed for connecting two minima on a potential energy surface (PES) and locating the associated transition state (TS) using only the first derivatives. The method operates two images starting from the initial and the final states, respectively, to walk in a stepwise manner toward each other. The surface walking involves repeated bias potential addition and local relaxation with the constrained Broyden dimer method to correct the walking direction. We apply the method to a model PES, a large set of gas phase Baker reactions, and complex surface catalytic reactions, which demonstrates that the DESW method can establish a low energy pathway linking two minima even without iterative optimization of the pathway, from which the TS can be located readily. By comparing the efficiency of the new method with the existing methods, we show that the DESW method is much less computationally demanding and is applicable for reactions with complex PESs. We hope that the DESW method may be integrated with the PES sampling methods for automated reaction prediction.

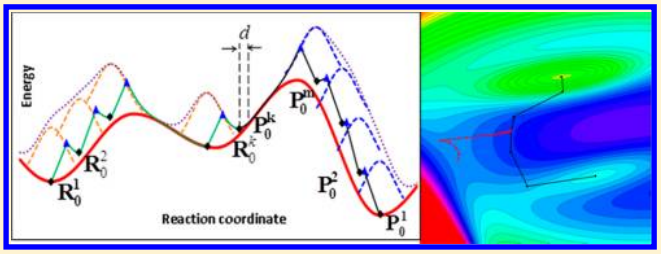

1. INTRODUCTION

The determination of the transition state (TS) of a chemical reaction and the reaction pathway on a potential energy surface (PES) is a main theme in theoretical chemistry, which is a key technique to predict reaction kinetics. In general, according to their starting structure and the input reaction coordinate (a vector leading to the target reaction), the TS-searching methods may be distinguished as two types. The single-ended methods often involve preguessing the TS-like structure and/or the reaction coordinate.[1−4] By contrast, the double-ended methods are more widely utilized in complex systems, for example, those encountered in catalytic reactions on the surface, solid−solid phase transition, and surface reconstruction, where the reaction coordinate is not intuitive, while the initial state (IS) and final state (FS) are known. The reaction coordinate is identified either using the information on a Hessian (the second derivatives of energy with respect to the coordinate) or involving iterative full pathway optimization.[5−15] It has been a long-standing challenge to improve the double-ended method for TS location without recourse to Hessian computation or accurate pathway determination.[6−9]

Most current double-ended methods,[5] for example the string method,[10,11] the growing string method,[12] and the nudged-elastic-band (NEB) method,[13−15] are methods targeted at identifying (or get an idea of) the reaction pathway (RP) that links two minima on a PES. The TS as the saddle point in the RP can be located during the pathway building, e.g., climbing image NEB (CI-NEB), or searched accurately after the pathway is built.[16−18] The overall efficiency of such double-ended methods could be quite sensitive to the initial guess pathway from IS to FS, e.g., obtained using linear interpolation. Ideally, the initial pathway should not be too far away from the RP, and meanwhile the interpolated points along the pathway should be dense enough to ensure the proper sampling at the TS regions and the convergence of the whole pathway. Some other methods such as the linear synchronous transit (LST)[19] using the internal coordinate and the quadratic synchronous transit (QST)[20] interpolation may be used to provide a better initial guess. The double-ended methods may suffer from "corner-cutting," "sliding-down," and TS convergence problems[15] (e.g., in the electronic structure calculations), especially when the RP is highly curved or deep valleys are present on the PES. A detailed account of TS-searching methods can be found in previous reviews.[5,21]

Recent years have seen the combination of TS-searching methods with other PES sampling techniques for automated pathway sampling to explore unknown reactions,[22−24] in which the PES sampling methods reveal the minima (i.e., IS/FS) and the TS-searching methods determine the TS and the pathway. It is therefore of significance to improve the efficiency and reliability of the double-ended methods for the reactivity prediction using large-scale computations. Recently, we developed a bias potential driven constrained-Broyden dimer (BP-CBD) method[25] for TS location using only the first derivatives (Hessian-free). The BP-CBD method is a single-ended method but does not need to preguess the TS-like structure. It starts from IS with a minimum requirement on the reaction information[25] (e.g., a pair of atoms related to the chemical bond making/breaking). One major feature of the BP-

Received: September 26, 2013
Published: November 14, 2013

dx.doi.org/10.1021/ct4008475 | J. Chem. Theory Comput. 2013, 9, 5745−5753

CBD method is the self-refinement of the reaction coordinate during the TS searching thanks to the biased CBD rotation. Inspired by this feature, here we develop a new double-ended surface walking method (DESW) for TS location starting from the known IS and FS.

The new DESW method can achieve the following: (i) to establish a low energy pathway in a noniterative way that mimics the RP at the regions close to the TS while allowing (large) deviation at the regions far away from the TS; (ii) to locate the TS efficiently using only the first derivatives without the need to preguess the reaction coordinate. Below, we will first present the algorithm of the DESW method and then apply the method to a model PES, a large set of gas phase Baker reactions, and catalytic reactions on surface. From these results, the main features, including the efficiency and the robustness of the method, are discussed by comparing with the existing double-ended method.

2. METHOD

The DESW method inherits important modules from the previous BP-CBD method, and these modules are modified accordingly to allow for the double-ended search. In the following, we will introduce the essence of the BP-CBD method and, on that basis, the algorithm of the DESW method is presented in detail.

2.1. Overview of BP-CBD Method. The BP-CBD method[25] contains three basic modules, namely, the biased rotation, the biased translation, and the constrained Broyden dimer (CBD) for TS location.[26] The biased rotation yields the normal mode ($\mathbf{N}$) pointing at the reaction direction, and the biased translation moves the image along the $\mathbf{N}$. By repeating the biased rotation and the biased translation, the image can gradually walk to the TS region starting from the IS. Once the curvature of $\mathbf{N}$ becomes negative (an indication of the TS region), the CBD module is called for to identify the TS exactly.

The biased rotation is a modification of the constrained Broyden dimer rotation method,[26] an algorithm to fast identify one softest normal mode of a Hessian for a structure ($\mathbf{R_0}$). The dimer is defined by two structural configurations, $\mathbf{R_1}$ and $\mathbf{R_0}$, separated by δR with the direction along the dimer being $\mathbf{N_t}$. In the biased rotation, a bias potential V_N is added onto the real PES V_{real}, and on this modified PES, a normal mode ($\mathbf{N_t}$ at convergence) is identified starting from an initial guess mode, $\mathbf{N_{init}}$, according to eqs 1−5. With the added bias potential, the biased rotation can locate the desired reaction direction instead of always converging to the softest mode. This is important, particularly at the minimum basin, where the interested reaction coordinate often associates with a normal mode with a large positive curvature (eigenvalue) and thus cannot be identified properly using the unbiased constrained Broyden dimer rotation.

$$V = V_{real} + V_N \tag{1}$$

$$V_N = -\frac{a}{2}[(\mathbf{R_1} - \mathbf{R_0})\cdot\mathbf{N_{init}}] = -\frac{a}{2}[\delta R(\mathbf{N_t}\cdot\mathbf{N_{init}})]^2 \tag{2}$$

$$\mathbf{F_N} = -\frac{\partial V_N}{\partial q} = a\delta R(\mathbf{N_t}\cdot\mathbf{N_{init}})\mathbf{N_{init}} \tag{3}$$

$$\begin{aligned}\Delta\mathbf{F}^{\perp} &= \Delta\mathbf{F}^{\perp}_{real} + \Delta\mathbf{F}^{\perp}_{\mathbf{N}} \\ &= 2(\mathbf{F_I} + \mathbf{F_N} - \mathbf{F_0}) - 2[(\mathbf{F_I} + \mathbf{F_N} - \mathbf{F_0})\cdot\mathbf{N_t}]\mathbf{N_t}\end{aligned} \tag{4}$$

$$C = C_{real} + C_N = C_{real} - a(\mathbf{N_t}\cdot\mathbf{N_{init}})^2 \tag{5}$$

As shown in eq 2, the bias potential V_N utilized in BP-CBD is a quadratic function with a parameter a that can be determined automatically during the rotation. The bias potential modifies the vertical force acting on the dimer (eq 4) and consequently affects the mode optimization. On convergence of the biased rotation, if the real curvature of the dimer, C_{real}, is negative, the CBD module is utilized to locate the TS; otherwise, the biased translation is continued to move the structural image toward TS.

The biased rotation only passes the normal mode to the biased translation, which is labeled as $\mathbf{N_i}$ with the subscript $\mathbf{i}$ standing for the sequence number of the Gaussian bias potential added. In brief, the biased translation is a repeated bias potential addition and local relaxation process to push a structure in a stepwise manner away from the minimum basin and simultaneously relax it down to the low energy region on the PES. The biased translation utilizes eqs 6−9 to add a Gaussian bias potential centering at a starting structure $\mathbf{R_0}^{\mathbf{i}}$, to translate the structure ($\mathbf{R_t}^{\mathbf{i}}$) uphill toward the TS region and to perform local relaxation to reach $\mathbf{R_0}^{\mathbf{i+1}}$. $\mathbf{R_0}^{\mathbf{i}}$ labels a series of local minima along the pathway created by adding Gaussian potentials on the real PES.

$$V = V_{real} + V_G \tag{6}$$

$$V_G = \sum_{i=1}^{k} v_i = \sum_{i=1}^{k} w_i \exp\left(-\frac{[(\mathbf{R_t}^{\mathbf{i}}\text{-}\mathbf{R_0}^{\mathbf{i}})\cdot\mathbf{N_i}]^2}{2ds^2}\right) \tag{7}$$

$$\mathbf{F} = \mathbf{F_{real}} + \mathbf{F_G} \tag{8}$$

$$\begin{aligned}\mathbf{F_G} &= -\frac{\partial V_G}{\partial q} \\ &= \sum_{i=1}^{k} \frac{w_i}{ds^2} \exp\left(-\frac{[(\mathbf{R_t}^{\mathbf{i}}\text{-}\mathbf{R_0}^{\mathbf{i}})\cdot\mathbf{N_i}]^2}{2ds^2}\right)[(\mathbf{R_t}^{\mathbf{i}}\text{-}\mathbf{R_0}^{\mathbf{i}})\cdot\mathbf{N_i}]\mathbf{N_i}\end{aligned} \tag{9}$$

As shown in eq 7, the biased potential V_G is a series of Gaussian functions, each defined by the width ds, the height w, and the normal mode $\mathbf{N_i}$ from the biased dimer rotation. The idea of the basin filling is similar to that in metadynamics.[27−29] The Gaussian height w is decided automatically in the translation, which must let $\mathbf{F}_0^i\cdot\mathbf{N}_i > 0$ to generate a proper local minimum on the modified PES. The Gaussian ds is a critical parameter defining the step size of the climbing and is typically around 0.1 Å for the TS search. On exit of the biased translation, a new local minimum $\mathbf{R_0}^{\mathbf{i+1}}$ is obtained on the modified PES. The biased rotation will be used to find the normal mode at $\mathbf{R_0}^{\mathbf{i+1}}$, which starts the new cycle by incrementing $\mathbf{i}$. The detailed algorithm of the BP-CBD method could refer to the previous work.[25,26]

2.2. Double-Ended Surface Walking Method. Different from the BP-CBD method, the DESW method defines one more structure image walking on PES, labeled as $\mathbf{R}$ and $\mathbf{P}$ starting from the IS basin and the FS basin, respectively, as illustrated in Figure 1. Similarly, the superscript $\mathbf{i}$ in Figure 1 indicates the sequence number of the Gaussian bias potential added on each side, and $\mathbf{R_0^i}$ and $\mathbf{P_0^i}$ refer to the local minima on the modified PES along the pathway, where the Gaussian functions are centered. The walking of the two structural images is described as follows (also see Figure 1). We start from the IS ($i = 1$), i.e., $\mathbf{R}_0^1$, getting the $\mathbf{N_1^{init,R}}$ using eq 10, utilizing

dx.doi.org/10.1021/ct4008475 | J. Chem. Theory Comput. 2013, 9, 5745−5753

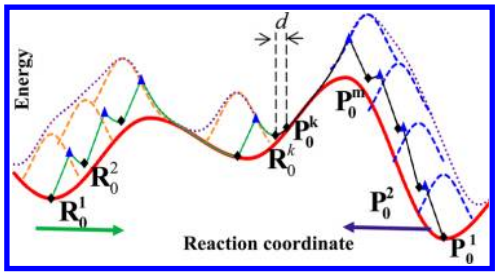

Figure 1. An illustration of the DESW method in 1D-PES, showing that two structure images starting from the IS and the FS sides walk toward each other (the arrow direction). The red, orange/blue, purple, and green/black curves represent the real PES (V_{real}), the Gaussian functions (v_i, i = 1, 2, ...k) at the IS/FS side, the modified PES, and the DESW trajectory, respectively. The local minima on the modified PES along the trajectory are labeled to be $\mathbf{R}_0^i/\mathbf{P}_0^i$, as indicated by a black diamond.

the biased rotation and the biased translation to reach $\mathbf{R}_0^2$. We then switch to the FS side and similarly reach $\mathbf{P}_0^2$ from $\mathbf{P}_0^1$, with eq 11 for generating $\mathbf{N}_1^{init,P}$. The whole process is repeated by incrementing **i**. The two images thus walk toward each other in an alternative manner ($\mathbf{R}_0^1 \rightarrow \mathbf{P}_0^1 \rightarrow \mathbf{R}_0^2 \rightarrow \mathbf{P}_0^2$...). The process terminates until they meet, i.e. the distance of the two images is below a threshold (set as 0.2 Å in this work). Once the pathway building is complete, a chain of structural images constituted by the local minima, $\mathbf{R}_0^i$ and $\mathbf{P}_0^i$, is obtained. Finally, we select the highest energy image (e.g., $\mathbf{P}_0^m$ in Figure 1) from the chain and utilize the CBD method[26] to locate the TS exactly. Note that apart from the CBD method, other single-ended methods may be used to locate the TS at this stage, such as Quasi-Newton methods[30] and eigenvalue-following methods[31,32] (if Hessian is cheaply available).

Obviously, the walking of the image from each side (**R** or **P**) is quite similar to that utilized in the BP-CBD method, i.e., via repeated biased rotation and biased translation, although the initial mode is generated differently. For the DESW method, the initial mode $\mathbf{N}_i^{init}$ is updated using eqs 10 and 11, and the converged $\mathbf{N}_i$ then provides the walking direction: $\mathbf{N}_i^{init,R}$ at the $\mathbf{R}_0^i$ points to $\mathbf{P}_0{}^i$; $\mathbf{N}_i^{init,P}$ at the $\mathbf{R}_{FS}{}^i$ points to $\mathbf{R}_0{}^{i+1}$. During the surface walking, the initial mode is not kept constant but changes continuously as the distance between $\mathbf{R}_0^i$ and $\mathbf{P}_0{}^i$ reduces. In such a way, the two walking images will meet eventually (as long as the Gaussian *ds* is not too small) and the desired reaction channel can be identified even without the iterative optimization of the whole pathway (see examples in section 3).

$$\mathbf{N}_i^{init,R} = \frac{\mathbf{P}_0{}^i - \mathbf{R}_0{}^i}{||\mathbf{P}_0{}^i - \mathbf{R}_0{}^i||} \tag{10}$$

$$\mathbf{N}_i^{init,P} = \frac{\mathbf{R}_0{}^{i+1} - \mathbf{P}_0{}^i}{||\mathbf{R}_0{}^{i+1} - \mathbf{P}_0{}^i||} \tag{11}$$

While the basic scheme of the DESW method is straightforward, its efficiency and robustness for finding the desired TS can depend on the value of Gaussian width *ds*. We found that a large *ds* can speed up the pathway building but may lead to a poor sampling at the TS region (passing over TS) and even the failure of the TS location, particularly when the TS has a large negative curvature (sharp peak). From Figure 1, it is clear that once the tail of added Gaussian potentials spans over the TS, the local relaxation may lead to the structural image converging rapidly to the bottom of the neighboring basin. As a result, few structural images as the local minima along the pathway can be close to the TS, and this increases the difficulty for the subsequent CBD method to locate the TS. In order to amend this problem, we have modified the original biased rotation and the biased translation of the BP-CBD method, as outlined in the following.

First, at the TS region, the unbiased rotation (without the bias potential) is utilized to refine the normal mode. At the TS region where a negative mode is present, it is in fact no longer necessary to add bias potential (eq 1), since the negative mode associated with the reaction is now the softest eigenvalue of the Hessian and can be identified correctly using unbiased rotation. Therefore, while the biased rotation is utilized initially, we will examine the real curvature of the dimer, C_{real} (eq 5), during the biased rotation: If C_{real} is negative, the unbiased CBD rotation will be performed to converge the negative normal mode.

Second, a constrained optimization is utilized for the local relaxation in the biased translation whenever the presence of a possible TS is detected. Conditional logic as written in eq 12 is utilized to examine whether the local relaxation may already pass over a TS:

$$\mathbf{F}_{0,real}^i \cdot \mathbf{N}_i < 0;\ \mathbf{F}_{real} \cdot \mathbf{N}_i > 0 \tag{12}$$

where $\mathbf{F}_{0,real}^i$ is the real force at the local minimum $\mathbf{R}_0^i$ (or $\mathbf{P}_0^i$), and $\mathbf{F}_{real}$ is the real force of the structure during the local relaxation after the addition of the *i*th Gaussian. Since $\mathbf{F}_{0,real}^i \cdot \mathbf{N}_i < 0$ is always satisfied from the IS/FS to the TS, the $\mathbf{F}_{real} \cdot \mathbf{N}_i > 0$, if having appeared during the local relaxation, is a good indication that the current structure is already over the TS. Therefore, if the condition in eq 12 is true, we restart the local optimization from the previous step, and a constrained optimization is performed using only the reversed parallel force along $\mathbf{N}_i$ as expressed in eq 13.

$$\mathbf{F}_p = -(\mathbf{F}_{real} \cdot \mathbf{N}_i)\mathbf{N}_i \tag{13}$$

This helps to correct the optimization back to the TS region. The constrained optimization ends if the magnitude of the parallel force ($||\mathbf{F}_p||$) increases (a similar idea was used previously in the CBD method for finding TS[26]).

It should be pointed out that the basic idea of the DESW method is similar to the previous saddle method proposed by Müller and Brown[6] and its extensions such as the ridge method,[7] in the sense that all these methods involve two structures stepping toward each other from either side of the reactant and the product under certain constraints to correct the walking direction and to control the walking step size. These two structures always bracket the saddle point on the PES[6−9,33,34] and can lead to the accurate TS via either iterative optimization or using other single-ended methods (e.g., CBD utilized in the DESW method). Only an approximate pathway (pseudopathway[9]) is yielded on convergence, different from the other double-ended methods such as the NEB and String method.

We may further outline the major differences of these pseudopathway methods according to the imposed constraint conditions: (i) The walking direction. The previous methods generally do not compute the eigenvectors of the Hessian but find the reaction direction via constrained local energy minimization, e.g., via simplex method or direct optimization using the gradient perpendicular to the vector linking two previous images.[33] The DESW method computes one

eigenvector ($\mathbf{N}_i$) using the (un)biased dimer rotation and thus can converge quickly toward the desired reaction pathway even without iterative optimization of the pathway. (ii) The step size. The previous methods generally set a fixed step size as measured by geometrical distance and reduce the size on approaching the TS. For example, the Müller–Brown saddle method[6] utilizes a hypersphere to constrain the distance between the new and the previous structures, and the images along the pathway are spaced by a fixed preset distance. The DESW method utilizes a single parameter, i.e., the Gaussian width *ds* (not exactly a geometrical distance) to control the walking step, and the spacing of images along the pathway is not equal but depends on the local PES. On the flat region of the PES, the DESW method can walk fast as driven by the tail of Gaussian functions.

2.3. The Overall Scheme of the DESW Method. A flowchart of the DESW method is summarized in Scheme 1, which is explained as follows.

Scheme 1. The Flow Chart of the DESW Method

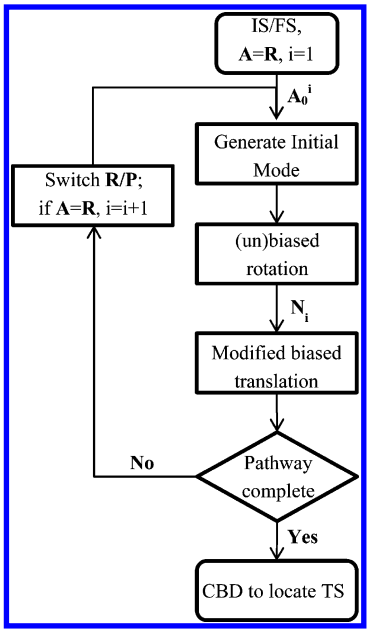

(i) The IS and FS structures, $\mathbf{R}_0^1$ and $\mathbf{P}_0^1$, are provided as input, and let $i = 1$ and $\mathbf{A} = \mathbf{R}$.
(ii) Generate the initial mode $\mathbf{N}_i^{\text{init,A}}$ at $\mathbf{A}_0^i$ using eq 10 ($\mathbf{A} = \mathbf{R}$) or 11 ($\mathbf{A} = \mathbf{P}$).
(iii) Utilize the biased rotation to identify the normal mode, $\mathbf{N}_i^A$. If $C_{\text{real}} < 0$, the unbiased rotation is used to further converge $\mathbf{N}_i^A$.
(iv) Utilize the biased translation to drag $\mathbf{A}_0^i$ to $\mathbf{A}_0^{i+1}$. If the condition in eq 12 is true during the local relaxation, the constrained optimization is performed instead with the force expressed in eq 13.
(v) Judge whether the pathway building is completed according to the distance between the two images. If the distance is below 0.2 Å, continue with the step vi; else return back to step ii by switching $\mathbf{A} = \mathbf{R}/\mathbf{P}$ and incrementing $\mathbf{i}$ when $\mathbf{A} = \mathbf{R}$.
(vi) Select the highest energy structure ($\mathbf{A}_0^m$) from the local minima chain and utilize the CBD method to locate TS exactly.

3. RESULTS AND DISCUSSION

3.1. 2-D Model PES: Wolfe–Quapp Function. To illustrate how the DESW method works, we first apply it to the 2-D function[12,35] Wolfe–Quapp (WQ) PES (eq 14), a well-studied model system for testing the efficiency of TS searching methods.[36−38] The contour map of the WQ PES is shown in Figure 2, in which the three minima, IS, MS, and FS, and the three TSs, TS1, TS2, and TS3, are labeled. The two most stable minima, IS and FS, can be connected via two possible minimum energy pathways, passing through either TS1–MS–TS3 or TS2, both being far away from the straight line linking the two minima. The major goal of the double-ended methods for TS location should be able to identify TS1 or TS2 provided with IS and FS. The TS1 is the highest energy point along the lowest energy pathway linking IS and FS and is thus of more interest in kinetics.

$$E(x, y) = x^4 + y^4 - 2x^2 - 4y^2 + xy + 0.3x + 0.1y \quad (14)$$

We found that the DESW method can identify both TS1 and TS2 starting from IS and FS by varying the Gaussian *ds*. The two DESW pathways are shown in Figure 2a. The left-hand curve passing TS1–MS–TS3 is obtained using the Gaussian *ds* = 0.4 for both sides, and the right-hand one passing TS2 is with

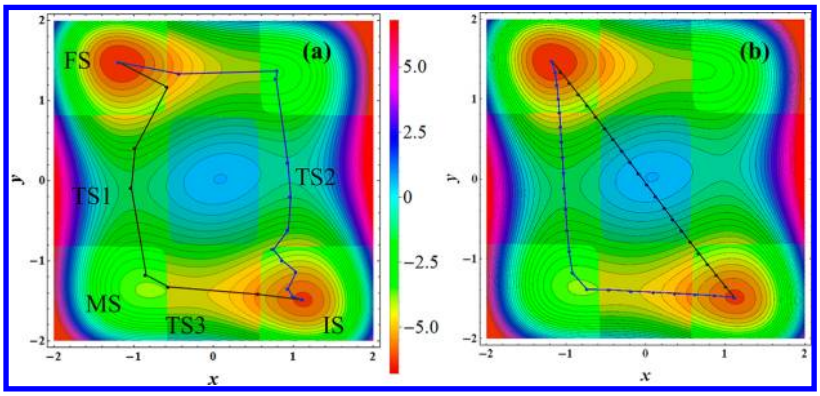

Figure 2. The DESW pathways (a) and the CI-NEB pathway (b) on the WQ PES. The shaded areas indicate the regions with the negative modes: two negative modes at the central region and only one negative mode on the other shaded area. The two DESW pathways are with different *ds* parameters (left, *ds* = 0.4/0.4; right, *ds* = 0.1/0.4, also see text). The initial interpolated line for CI-NEB is also shown in b.

dx.doi.org/10.1021/ct4008475 | J. Chem. Theory Comput. 2013, 9, 5745−5753

ds = 0.1 from the IS side and 0.4 from the FS side. We notice that TS1 is identified more frequently by performing the DESW calculations with a different choice of *ds*. While, in principle, one can tune the *ds* to sample different pathways when multiple reaction channels are present to connect IS and FS, the parameter tuning is however not practical in first principles calculations. In general, we found that *ds* = 0.1−0.2 Å, equal at both sides, is a good choice for typical chemical reactions.

For comparison, the CI-NEB method[17] is also performed to search the TS on the WQ PES starting from the same IS and FS, as implemented in the VTST Tools package.[39] The CI-NEB search starts from a 20-image straight line interpolated between IS and FS (blue line) and converges to its closest minimum energy pathway that is the lowest energy pathway (purple curve) after 164 iterations. The CI-NEB results are shown in Figure 2b. The fifth and 12th images are converged to the TS3 and the TS1, respectively.

To further illustrate the performance of the DESW method in complex PES, a 2-D model PES with highly curved MEP is constructed (modified from Müller−Brown PES[6]) featured with a ridge separating two divergent reaction valleys, as shown in Figure 3. In this case, the straight line connecting the IS and

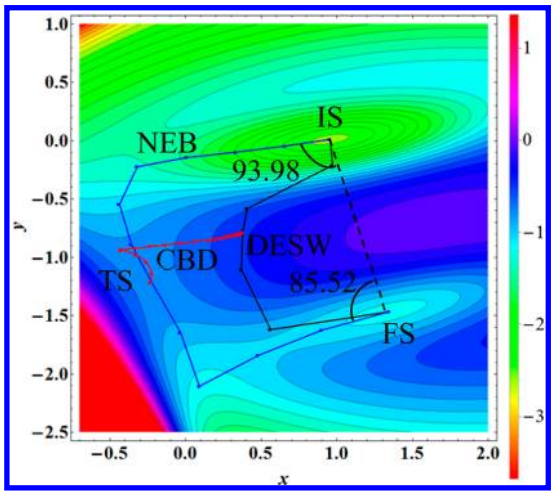

Figure 3. The DESW trajectory on a 2-D PES (modified from Müller−Brown PES[6]) with the feature that a ridge separates two divergent reaction valleys. DESW: the DESW pathway (*ds* 0.2). CBD: the CBD trajectory in the DESW search. NEB: the converged CI-NEB trajectory (a mimic of MEP).

FS has a large angle (around 90°) with respect to the initial MEP direction, and the previous double-ended saddle methods fail on such a PES.[6] We found that the DESW method can successfully identify the correct TS even for such reactions with a highly curved pathway. As shown, the DESW links quickly IS and FS to yield a curved pathway, and the CBD method then identifies the correct TS from the highest energy image of the DESW pathway. The success of the DESW method for TS location, despite its noniterative behavior in the pathway building, can be attributed to the following two main reasons. First, the walking direction utilized in DESW is the one born from the (un)biased dimer rotation: the biased rotation can bias the direction toward the IS−FS intermediate region and simultaneously pointing toward the TS regions. This effectively takes into account the essential reaction information from the Hessian. Second, the single-ended CBD method is further utilized to refine the TS, which is particularly useful for the highly curved pathway system, where the noniterative pathway building cannot provide a good reaction pathway.

By comparing the results from the DESW method with those from the CI-NEB method, we can outline the major features of the DESW method. (i) The DESW pathway grows gradually starting from the IS/FS and does not require an initial pathway guess, e.g., the linear interpolation in between IS and FS. The knowledge of IS/FS is cast into the reaction direction, which is refined as a normal mode by the biased rotation. The method avoids the predefinition of the total number of images along the pathway and eliminates the possibility of running into unrealistic high energy states on the PES (e.g., the middle region in the WQ PES). (ii) The DESW method can locate the TS even without the iterative optimization of the whole pathway. Since the iterative pathway optimization in the NEB method is to identify correctly the reaction coordinate defined by the connectivity of neighboring images, such a procedure is no longer essential because the (un)biased rotation is utilized to correct the reaction direction in the DESW search. Although the DESW pathway may deviate largely from the minimum energy pathway near the IS and the FS basins, it can identify quickly the entrance channel to the TS and sample the TS region properly.

We would like to emphasize that the optimization of the whole pathway for the purpose of TS location may not be worthwhile since the computational efforts could be dominated by the cost to converge structures that are far away from the TS. On the other hand, the RP can always be retrieved, if interested, using the obtained TS with alternative techniques, such as the intrinsic reaction pathway (IRC) using the Gonzalez−Schlegel method[40] and the Ishida−Morokuma−Komornicki (IMK) method.[41]

3.2. Baker Reactions. Next, we move on to real reactions to examine the performance of the DESW method. Here, we utilize the Baker reactions[42] as the model system, a benchmark set for the TS location of gas phase reactions,[43] and these reactions were previously utilized by us to analyze the BP-CBD method.[25] We utilize the density functional theory (DFT) SIESTA package[44] to evaluate the energy/force of these reactions. The exchange-correlation functional is GGA-PBE,[45] and the basis set is numerical atomic basis (NAO) with double-ζ polarization.[46,47] We have examined the performance of the DESW method with two different sets of *ds* parameters, namely 0.1 and 0.2 Å (*ds* is kept the same for both sides). The convergence criterion for biased rotation is 0.1 eV/Å for the rotational force (eq 4), and the TS is considered to be reached when the maximum force per degree of freedom is below 0.1 eV/Å. All the located TSs have been checked and confirmed by comparing with our previous work and the literatures.

For comparison, we also utilized the CI-NEB method for locating the same Baker reactions. Eight images are linearly interpolated from the Cartesian coordinates of the IS and the FS to yield the initial NEB pathway, and the fast inertial relaxation engine (FIRE) method[48] is utilized as the optimizer.[39] The spring constant of NEB is set as 5.0 eV/Å, and all the other parameters are the same as that used in ref 48. The numerical results from the DESW methods and the CI-NEB method for locating the TSs are shown in Table 1, highlighting the total energy/force evaluation steps.

Table 1 shows that the DESW method reduces significantly the total energy/force evaluation steps to locate TS compared to the CI-NEB method (note that CI-NEB method can run in

Table 1. Results of the DESW method for TS location of Baker reactions.[42]

				ds 0.1[c]				*ds* 0.2[c]			
no.	reaction	dist[a]	tot (NEB)[b]	nG	tot	rot/trans/CBD	TS-dist[d]	nG	Tot	rot/trans/CBD	TS-dist[d]
1	HCN → HNC	2.05	568	12	209	88/117/4	0.00	6	127	50/66/11	0.10
2	HCCH → CCH_2	1.70	376	10	123	56/61/6	0.04	6	82	38/39/5	0.02
3	H_2CO → H_2+CO	2.19	576	16	228	106/114/8	0.40	10	170	72/90/8	0.50
4	CH_3O → CH_2OH	1.36	376	9	163	62/81/20	0.15	6	110	47/44/19	0.27
5	ring-opening cyclopropyl	2.34	552	15	211	89/97/25	0.61	9	176	55/69/52	0.73
6	bicyclo110 butane TS2	2.52	624	15	183	86/85/12	0.54	9	128	50/64/14	0.67
7	*β*-(formyloxy) ethyl	1.99	800	13	217	94/80/43	0.55	8	125	56/54/15	0.48
8	parent Diels–Alder	1.66	632	14	150	84/63/3	0.00	14	108	60/41/7	0.06
9	s-tetrazine →2HCN + N_2	2.53	504	15	227	101/109/17	0.24	10	196	84/90/22	0.35
10	rotational TS in butadiene	4.43	520	18	259	94/161/4	0.00	14	195	78/114/3	0.00
11	H_3CCH_3 → H_2CCH_2+H_2	2.57	688	21	286	132/147/7	0.09	12	194	76/100/18	0.28
12	H_3CCH_2F → H_2CCH_2+ HF	2.02	368	13	219	88/115/16	0.13	7	115	40/54/21	0.25
13	H_2CCHOH → H_3CCHO	2.31	536	16	236	101/119/16	0.17	8	153	76/67/10	0.23
14	HCOCl → HCl + CO	2.05	392	12	166	63/91/12	0.17	7	110	43/60/7	0.16
15	H_2O+PO_3^- → $H_2PO_4^-$	2.39	640	14	197	88/95/14	0.29	9	162	77/61/24	0.36
16	Claisen rearrangement	2.14	408	13	217	107/97/13	0.09	12	139	62/66/11	0.16
17	silylene insertion	2.11	424	12	161	73/83/5	0.04	9	96	43/47/6	0.06
18	HNCCS → HNC + CS	2.84	704	12	181	88/90/3	0.00	8	215	71/74/70	0.51
19	$HCONH_3^+$ → NH_4^+ + CO	2.35	440	18	266	121/133/12	0.28	11	186	75/82/29	0.48
20	rotational TS in acrolein	3.11	576	13	224	95/125/4	0.00	10	158	79/74/5	0.01
21	HCONHOH → HCOHNHO	1.91	568	12	200	93/97/10	0.06	7	127	62/53/12	0.23
22	HNC + H_2 → H_2CNH	2.50	736	16	223	102/104/17	0.31	13	257	102/119/36	0.38
23	H_2CNH → $HCNH_2$	1.84	1112	9	140	49/84/7	0.10	5	98	35/53/10	0.12
24	$HCNH_2$ → HCN + H_2	2.30	648	15	229	99/103/27	0.59	12	207	76/89/42	0.92
	average	2.30	574	14	205	90/102/13	0.20	9	151	63/70/19	0.30

[a]The Euclidean distance (Å) between IS and FS, $\|\mathbf{R}_{IS} - \mathbf{R}_{FS}\|$. [b]The energy/force evaluation steps summed over all eight NEB images. [c]nG: the number of Gaussians added. Tot: the total force/energy evaluation steps. Rot/Trans/CBD: the force/energy evaluation steps in the dimer rotation, biased translation, and CBD of TS location, respectively, for DESW calculations. [d]TS-dist: The Euclidean distance (Å) between the guessed TS (maximum energy structure) from the DESW pathway and the located TS from CBD.

parallel and the actual timings are quite similar for both methods provided with enough computational resources). For the DESW method, the increase of *ds* from 0.1 to 0.2 can reduce the average total force/energy evaluation steps by 24% (from 205 steps to 151 steps). The average number of Gaussians added along the pathway (average image number) in the DESW pathway is related to the choice of *ds*. It is 14 for *ds* = 0.1 and nine for *ds* = 0.2 Å. The latter is close to that (eight) utilized in the CI-NEB method. Therefore, we can attribute the high efficiency of the DESW method to its noniterative behavior of pathway building, not the reduced number of images along the pathway.

Compared to the single-ended BP-CBD method (~100 steps for Baker reactions),[25] we noted that the DESW method for TS location is less efficient, as expected. These two methods are within the same theoretical framework, i.e., similar surface walking, and the same CBD method for TS location, and the BP-CBD only involves the surface walking from one side. One should bear in mind that the double-ended method is advantageous for complex reactions when the reaction coordinate is not intuitive.

Table 1 also shows the energy/force evaluation steps spent in the three major modules, i.e., the biased rotation, the biased translation, and the CBD for TS location, in the *ds* = 0.1/0.2 set DESW calculations. In general, the DESW method spends most of its time in building the pathway (>90%). This indicates that the guessed TS-like structure from the DESW pathway is already close to the true TS, from which the CBD can locate the TS readily, as quantified by the Euclidean distance between the guessed TS-like structure from the DESW pathway and the located TS from CBD (TS-dist in Table 1). The smaller *ds* set can provide a better guessed TS-like structure for CBD but is at the expense of the effort in building the pathway. In the pathway building, the energy/force steps spent on the biased rotation and the biased translation are roughly equal.

By comparing the results of *ds* being 0.1 and 0.2, we notice that while *ds* 0.2 generally reduces the overall time for TS location, the opposite cases are present, e.g., HNCCS → HNC + CS (no. 18 in Table 1) and HNC + H_2 → H_2CNH (no. 22 in Table 1). In these two reactions, the CBD steps are significantly large, which leads to the overall poorer performance for *ds* = 0.2 compared to *ds* = 0.1. We emphasize that although the efficiency of the DESW method is related to the *ds* parameter, the overall efficiency with respect to TS identification is in fact not very sensitive; namely, there is an optimum region of *ds* values, e.g. 0.1–0.2 (Å) for most reactions investigated. When the *ds* is small, the cost to build the pathway as measured by the force evaluation times will be dominant (too slow in the surface walking). By contrast, when the *ds* is large, the cost to locate TS using CBD could turn out to be significant because of the poor sampling at the TS region (bypassing the TS peak).

To provide a deeper insight into the efficiency difference between the DESW method and the CI-NEB method, we have selected two representative reactions for the pathway analysis, namely, CH_3O → CH_2OH (no. 4 in Table 1) and H_2CNH → $HCNH_2$ (no. 23 in Table 1). We plotted the trajectories obtained from the DESW method and the CI-NEB method for these two reactions in Figure 4, together with the IRC pathway

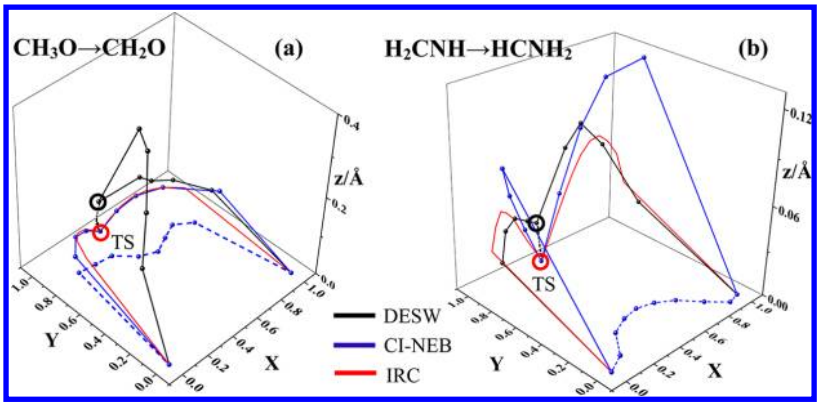

Figure 4. The DESW trajectory (ds = 0.1), the CI-NEB pathway, and the IRC pathway for $CH_3O \rightarrow CH_2OH$ (a) and $H_2CNH \rightarrow HCNH_2$ (b). Black: the DESW trajectory, including the pathway (solid) and the CBD trajectory to locate TS (dotted). Blue: the CI-NEB pathways after the first iteration (dotted) and on the convergence (solid). Red: the calculated IRC pathway. The TS is indicated by the red circle, and the structure where DESW starts to use CBD method to locate TS is indicated by the black circle.

obtained using the Gonzalez–Schlegel IRC method.[40] In these plots, the unit vectors **X** and **Y** are defined in eqs 15 and 16, and the z value can be calculated using eq 17. By definition, the X axis is the reaction coordinate, the Y axis represents the structural deviation from the reaction coordinate by projecting the structure onto the IS–TS–FS plane, and the Z axis represents the structural deviation out of the IS–TS–FS plane.

$$\mathbf{X} = \frac{\mathbf{R}^{FS} - \mathbf{R}^{IS}}{\|\mathbf{R}^{FS} - \mathbf{R}^{IS}\|} \tag{15}$$

$$\mathbf{Y} = \frac{\mathbf{R}^{TS} - \mathbf{R}^{IS} - [(\mathbf{R}^{TS} - \mathbf{R}^{IS})\cdot\mathbf{X}]\mathbf{X}}{\|\mathbf{R}^{TS} - \mathbf{R}^{IS} - [(\mathbf{R}^{TS} - \mathbf{R}^{IS})\cdot\mathbf{X}]\mathbf{X}\|} \tag{16}$$

$$z = \|(\mathbf{R} - \mathbf{R}^{IS}) - [(\mathbf{R} - \mathbf{R}^{IS})\cdot\mathbf{X}]\mathbf{X} - [(\mathbf{R} - \mathbf{R}^{IS})\cdot\mathbf{Y}]\mathbf{Y}\| \tag{17}$$

For the $CH_3O \rightarrow CH_2OH$ reaction, the total energy/force evaluation steps for the DESW method and the CI-NEB method are 163 (ds = 0.1) and 376, respectively; the ratio of them (163/376) is about the average number (205/574). In this reaction, Figure 4a shows that the initial CI-NEB pathway (dotted blue curve) is not far away from the converged CI-NEB pathway (solid blue curve), which is almost identical to the IRC pathway. The DESW pathway (solid black curve) has a large deviation initially at the IS basin but converges quickly to the IS–TS–FS plane at the fifth image ($\mathbf{R}_5^R$), from which the TS is located readily (dotted black curve).

For the $H_2CNH \rightarrow HCNH_2$ reaction, the DESW method (140 steps for ds = 0.1) performs similarly to the other reactions, but the CI-NEB method is frustrated to locate the TS (1112 steps). Figure 4b shows that the DESW pathway, despite its noniterative behavior, is quite close to the IRC pathway. By contrast, for the CI-NEB method, the initial CI-NEB string is far away from the IRC pathway, and thus extensive iterative optimization is required to converge the whole pathway in order to locate the TS. Even when the TS is reached, the CI-NEB pathway is still not properly converged to the IRC pathway (this could be due to the limited images utilized in building the pathway).

By comparing the DESW method with the CI-NEB method in Baker reactions, we found that the DESW method performs generally well for TS location and is not sensitive to the type of reactions. Owing to its noniterative behavior, the DESW method gains the overall efficiency of TS location but is at the expense of converging to the exact IRC pathway. In order to obtain the IRC pathway, additional calculations are needed to further optimize the pseudopathway, via either the obtained TS (e.g., IRC calculation) or the DESW pathway (e.g., pathway iteration using NEB method). On the other hand, the CI-NEB method could identify the TS and yield a pathway close to the IRC pathway in one go. The efficiency of the CI-NEB method is not high in general for the purpose of TS location and is also sensitive to the initial conditions, including the number of images and the initial pathway interpolation, which often requires a preknowledge of the reaction system.

3.3. Catalytic Reaction on Surface. Finally, we have applied the DESW method to heterogeneous catalytic reactions on surfaces. Here, a CO+OH → COOH on Pt(111) is selected as the model reaction, which is an important elementary step in many applications, such as the water–gas shift reaction,[49−52] and in electrocatalysis of alcohols.[4] The reaction involves a CO molecule reacting with a OH group, both adsorbed on top sites of Pt(111). The standard periodic DFT slab calculations as implemented in SIESTA have been carried out to investigate the reaction, where a four layer slab of Pt(111) with the bottom two layers is fixed at the bulk-truncated position. The supercell utilized is a $3 \times \sqrt{3}$ slab (six Pt atoms per layer), and a Monkhorst–Pack k-point ($2 \times 4 \times 1$) sampling is utilized. The other calculation details are the same as in our previous work.[53]

For catalytic reactions on the surface, the reactants often need to diffuse on the surface before they react, and therefore it is common that multiple TSs are present along a pathway, including both diffusion TSs and the chemical bond making/breaking TS. To test the performance of the DESW method, we have adopted two different sets of IS/FS with different separation distances between the CO and OH. In the first set of IS/FS (IS1 and FS1), the CO and the OH adsorb at the neighboring top sites with the distance OC–OH being 3.05 Å (IS1). The CO and OH can react to form COOH straightforwardly (without diffusion). In the second set (IS2 and FS2), the CO and OH are separated by 5.00 Å (IS2), and the reaction to form COOH requires the diffusion of the reactants. In all the calculations, we set the Gaussian ds as 0.2 Å. Our results for the DESW trajectories, including the pathway and the CBD trajectory, are plotted in Figure 5 together with the IRC pathway calculated using the IRC method.[40] The total energy/force evaluation steps are 261 in Figure 5a (210 and 51

dx.doi.org/10.1021/ct4008475 | J. Chem. Theory Comput. 2013, 9, 5745−5753

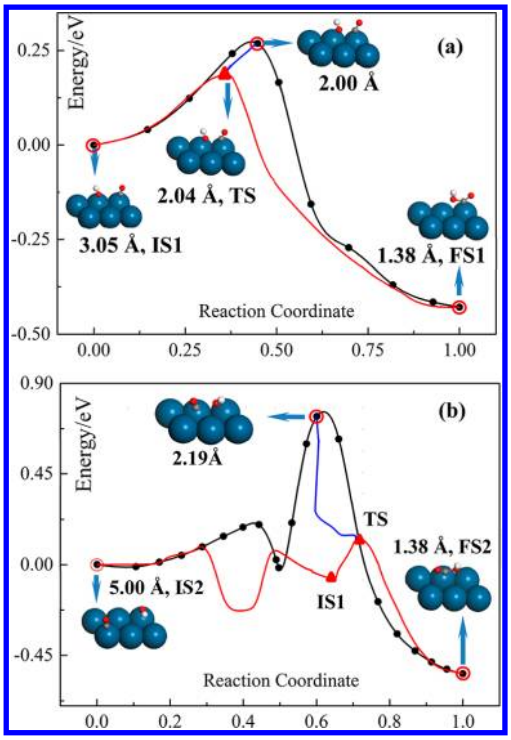

Figure 5. The DESW trajectories to locate the TS of the CO+OH → COOH reaction on Pt(111), with *ds* being 0.2 Å. Black and blue: the DESW trajectory, including the pathway (black) and the CBD trajectory (blue) to locate the TS. Red: the IRC pathway from the IRC method. The OC−OH distance is indicated together with the structure snapshots.

steps for building the pathway and to locate the TS, respectively) and 483 steps in Figure 5b (343 and 140 steps).

As shown, the DESW method can identify correctly the bond making TS of the CO+OH reaction in both cases since the highest energy image along the pathway always relates to the OC−OH bond formation. The calculated barrier is 0.18 eV with respect to the IS1, the CO and OH coadsorbed at the neighboring sites.

Figure 5 shows that the efficiency for TS location using the DESW method will depend on the type of reaction, a single-step or multistep reaction. For the elementary reaction, as shown in a, the obtained DESW energy profile is quite close to that of the IRC pathway, and the highest energy image along the chain is already a good approximation of the TS (the distance of OC−OH differs by 0.04 Å). By contrast, for the multistep reaction, as shown in b where both the surface diffusion and bond formation are involved, the DESW pathway can have a large deviation from the IRC pathway, not least because the IS2 and the FS2 are too far apart and the initial guess of reaction direction is poor. Specifically, the highest energy image along the chain deviates from the TS (the distance of OC−OH differs by 0.15 Å), and the DESW pathway does not capture accurately the lowest energy CO diffusion, where two additional TSs are present for CO diffusion from one top site to another (see the IRC pathway). In this particular case, extra iterations are desirable to optimize the pathway in order to confirm the energy maximum along the pathway, although the CBD method locates the correct TS using the DESW pathway in Figure 5b. This can be done, e.g., by decomposing the reaction into three elementary steps, each described by one individual DESW pathway.

From the examples shown above, we demonstrate that the DESW method can be an efficient and reliable tool for connecting two minima on complex PES and locating the TS. Because of the consecutive bias potentials added, the method can overcome a high barrier or go through a deep valley on the PES. The pathway building is facile to converge owing to its noniterative behavior with a self-corrected reaction coordinate. In practice, it is convenient to utilize DESW as a first tool to probe the pathway between IS and FS, especially when the reaction mechanism is unknown and the reaction may contain multiple elementary steps, exhibiting a complex PES. The saddle points and the intermediate minima can be located from the images along the DESW pathway as a post processing using other techniques (e.g., CBD utilized here for finding TS), from which the reaction kinetics can be derived. Our ongoing work shows that the DESW method can be integrated readily with the PES sampling method, i.e., our recently proposed stochastic surface walking (SSW) method,[54,55] in one unified theoretical framework for automated pathway searching toward the activity prediction of chemical reactions. The SSW method explores the PES exhaustively to provide closely connected minima pairs, and the DESW method refines the SSW trajectory and helps to resolve the reaction kinetics by locating the TS.

4. CONCLUSION

This work develops a new double-ended method for TS location using only the first derivatives, namely the DESW method. By presenting the algorithm in detail and applying it to a number of gas phase and heterogeneous reaction systems, we demonstrate that the DESW method is, in general, an efficient and reliable method for connecting two known minima and locating the TS, featuring the self-corrected reaction coordinate and the noniterative pathway building.

The DESW method is the latest development in the family of PES exploration methods based on the constrained Broyden technique, which can be used to locate TS from a preguessed TS-like structure (CBM[4] and CBD[26] methods), a single minimum (BP-CBD method[25]), or two minima (current DESW method) and even to predict unknown structures from randomly distributed atoms (SSW method).[54,55] These methods share the common modules, such as the biased rotation, the biased translation, and the constrained Broyden optimizer (thus, new algorithms along the line can be implemented without extensive coding), but differ generally in the way of initial mode generation. Obviously, the design of a reasonable reaction mode plays a central role in PES exploration, both for TS searching and for the sampling of new minimum structures. The integration of these methods, in particular by combining the SSW method with the DESW method, would be an exciting new area to explore toward the automated activity prediction of complex reaction systems with the help of large-scale computations.

AUTHOR INFORMATION

Corresponding Author

*E-mail: zpliu@fudan.edu.cn.

Notes

The authors declare no competing financial interest.

ACKNOWLEDGMENTS

We acknowledge the National Science Foundation of China (21173051, 21361130019), 973 program (2011CB808500,

2013CB834603), Science and Technology Commission of Shanghai Municipality (08DZ2270500), and Program for Professor of Special Appointment (Eastern Scholar) at Shanghai Institute of Higher Learning for financial support.

REFERENCES

(1) Malek, R.; Mousseau, N. *Phys. Rev. E* **2000**, *62*, 7723−7728.
(2) Henkelman, G.; Jonsson, H. *J. Chem. Phys.* **1999**, *111*, 7010−7022.
(3) Cerjan, C. J.; Miller, W. H. *J. Chem. Phys.* **1981**, *75*, 2800−2806.
(4) Wang, H.-F.; Liu, Z.-P. *J. Am. Chem. Soc.* **2008**, *130*, 10996−11004.
(5) Koslover, E. F.; Wales, D. J. *J. Chem. Phys.* **2007**, *127*, 134102.
(6) Müller, K.; Brown, L. *Theor. Chim. Acta* **1979**, *53*, 75−93.
(7) Ionova, I. V.; Carter, E. A. *J. Chem. Phys.* **1993**, *98*, 6377−6386.
(8) Ionova, I. V.; Carter, E. A. *J. Chem. Phys.* **1995**, *103*, 5437−5441.
(9) Schlegel, H. B. *J. Comput. Chem.* **2003**, *24*, 1514−1527.
(10) E, W.; Ren, W.; Vanden-Eijnden, E. *Phys. Rev. B: Condens. Matter Mater. Phys.* **2002**, *66*, 052301.
(11) E, W.; Ren, W.; Vanden-Eijnden, E. *J. Phys. Chem. B* **2005**, *109*, 6688−6693.
(12) Quapp, W. *J. Chem. Phys.* **2005**, *122*, 174106.
(13) Elber, R.; Karplus, M. *Chem. Phys. Lett.* **1987**, *139*, 375−380.
(14) Henkelman, G.; Jonsson, H. *J. Chem. Phys.* **2000**, *113*, 9978−9985.
(15) Trygubenko, S. A.; Wales, D. J. *J. Chem. Phys.* **2004**, *120*, 2082−2094.
(16) Goodrow, A.; Bell, A. T.; Head-Gordon, M. *J. Chem. Phys.* **2008**, *129*, 174109.
(17) Henkelman, G.; Uberuaga, B. P.; Jonsson, H. *J. Chem. Phys.* **2000**, *113*, 9901−9904.
(18) Zimmerman, P. *J. Chem. Theory Comput.* **2013**, *9*, 3043−3050.
(19) Peng, C.; Schlegel, H. B. *Isr. J. Chem.* **1993**, *33*, 449−454.
(20) Halgren, T. A.; Lipscomb, W. N. *Chem. Phys. Lett.* **1977**, *49*, 225−232.
(21) Schlegel, H. B. *WIREs Comput Mol. Sci.* **2011**, *1*, 790−809.
(22) Wales, D. J. *Int. Rev. Phys. Chem.* **2006**, *25*, 237−282.
(23) Henkelman, G.; Jonsson, H. *J. Chem. Phys.* **2001**, *115*, 9657−9666.
(24) Maeda, S.; Ohno, K.; Morokuma, K. *J. Chem. Theory Comput.* **2009**, *5*, 2734−2743.
(25) Shang, C.; Liu, Z.-P. *J. Chem. Theory Comput.* **2012**, *8*, 2215−2222.
(26) Shang, C.; Liu, Z.-P. *J. Chem. Theory Comput.* **2010**, *6*, 1136−1144.
(27) Laio, A.; Parrinello, M. *Proc. Natl. Acad. Sci. U. S. A.* **2002**, *99*, 12562−12566.
(28) Alessandro, L.; Francesco, L. G. *Rep. Prog. Phys.* **2008**, *71*, 126601.
(29) Iannuzzi, M.; Laio, A.; Parrinello, M. *Phys. Rev. Lett.* **2003**, *90*, 238302.
(30) Burger, S. K.; Ayers, P. W. *J. Chem. Phys.* **2010**, *132*, 234110−234117.
(31) Baker, J. *J. Comput. Chem.* **1986**, *7*, 385−395.
(32) Banerjee, A.; Adams, N.; Simons, J.; Shepard, R. *J. Phys. Chem.* **1985**, *89*, 52−57.
(33) Cárdenas-Lailhacar, C.; Zerner, M. C. *Int. J. Quantum Chem.* **1995**, *55*, 429−439.
(34) Dewar, M. J. S.; Healy, E. F.; Stewart, J. J. P. *J. Chem. Soc., Faraday Trans. 2* **1984**, *80*, 227−233.
(35) Wolfe, S.; Schlegel, H. B.; Csizmadia, I. G.; Bernardi, F. *J. Am. Chem. Soc.* **1975**, *97*, 2020−2024.
(36) Aguilar-Mogas, A.; Gimenez, X.; Bofill, J. M. *J. Chem. Phys.* **2008**, *128*, 104102.
(37) Aguilar-Mogas, A.; Giménez, X.; Bofill, J. M. *J. Comput. Chem.* **2010**, *31*, 2510−2525.
(38) Bofill, J. M.; Quapp, W. *J. Chem. Phys.* **2011**, *134*, 074101.
(39) Henkelman, G.; Uberuaga, B.; Jónsson, H., http://theory.cm.utexas.edu/vasp/neb/ (accessed September 24, 2013).
(40) Gonzalez, C.; Schlegel, H. B. *J. Phys. Chem.* **1990**, *94*, 5523−5527.
(41) Ishida, K.; Morokuma, K.; Komornicki, A. *J. Chem. Phys.* **1977**, *66*, 2153−2156.
(42) Baker, J.; Chan, F. *J. Comput. Chem.* **1996**, *17*, 888−904.
(43) Heyden, A.; Bell, A. T.; Keil, F. J. *J. Chem. Phys.* **2005**, *123*, 224101.
(44) José, M. S.; Emilio, A.; Julian, D. G.; Alberto, G.; Javier, J.; Pablo, O.; Daniel, S.-P. *J. Phys.: Condens. Matter* **2002**, *14*, 2745.
(45) Perdew, J. P.; Burke, K.; Ernzerhof, M. *Phys. Rev. Lett.* **1996**, *77*, 3865−3868.
(46) Junquera, J.; Paz, Ó.; Sánchez-Portal, D.; Artacho, E. *Phys. Rev. B: Condens. Matter Mater. Phys.* **2001**, *64*, 235111.
(47) Anglada, E.; M. Soler, J.; Junquera, J.; Artacho, E. *Phys. Rev. B: Condens. Matter Mater. Phys.* **2002**, *66*, 205101.
(48) Bitzek, E.; Koskinen, P.; Gähler, F.; Moseler, M.; Gumbsch, P. *Phys. Rev. Lett.* **2006**, *97*, 170201.
(49) Grabow, L. C.; Gokhale, A. A.; Evans, S. T.; Dumesic, J. A.; Mavrikakis, M. *J. Phys. Chem. C* **2008**, *112*, 4608−4617.
(50) Zhai, Y.; Pierre, D.; Si, R.; Deng, W.; Ferrin, P.; Nilekar, A. U.; Peng, G.; Herron, J. A.; Bell, D. C.; Saltsburg, H.; Mavrikakis, M.; Flytzani-Stephanopoulos, M. *Science* **2010**, *329*, 1633−1636.
(51) Liu, Z.-P.; Jenkins, S. J.; King, D. A. *Phys. Rev. Lett.* **2005**, *94*, 196102.
(52) Tang, Q.-L.; Liu, Z.-P. *J. Phys. Chem. C* **2010**, *114*, 8423−8430.
(53) Fang, Y.-H.; Wei, G.-F.; Liu, Z.-P. *Catal. Today* **2013**, *202*, 98−104.
(54) Zhang, X.-J.; Shang, C.; Liu, Z.-P. *J. Chem. Theory Comput.* **2013**, *9*, 3252−3260.
(55) Shang, C.; Liu, Z.-P. *J. Chem. Theory Comput.* **2013**, *9*, 1838−1845.